CIRP Annals - Manufacturing Technology xxx (2016) xxx–xxx

Contents lists available at ScienceDirect

CIRP Annals - Manufacturing Technology

journal homepage: http://ees.elsevier.com/cirp/default.asp

A study on machining of binder-less polycrystalline diamond by femtosecond pulsed laser for fabrication of micro milling tools

Yoshinori Ogawa [a], Michiharu Ota [b], Kazuo Nakamoto [b], Tomohiro Fukaya [c], Marc Russell [b], Tarek I. Zohdi [b], Kazuo Yamazaki (1)[b,*], Hideki Aoyama [a]

[a] Keio University, Yokohama, Japan
[b] University of California, Berkeley, USA
[c] Sumitomo Electric Hardmetal Corporation, Itami, Japan

ARTICLE INFO

Keywords:
Laser beam machining
Diamond tool
Femtosecond pulsed laser

ABSTRACT

Since binder-less polycrystalline diamond (BLPCD) has no macro cleavage planes and highest hardness, it is desirable material for micro milling tools. However, fabricating micro tools made of BLPCD by conventional method such as grinding is very time consuming due to its extremely high hardness. This paper describes the successful results obtained in our recent study on productive machining of BLPCD using femtosecond-pulsed laser (FSPL). The ablation effect of BLPCD by FSPL has been studied by conducting a series of experiments. Also, the predictability of ablation effect of FSPL when machining BLPCD has been evaluated by introducing numerical analysis model.

1. Introduction

Binder-less polycrystalline diamond (BLPCD) was developed in 2003 [1] and was evolved as an extremely high performance tool material in 2012 for machining non-ferrous materials [2]. Since BLPCD has superior mechanical properties (high hardness, high wear resistance, isotropic mechanical strength, etc.) to that of conventional diamond materials such as single crystalline diamond (SCD) and binder containing polycrystalline diamond (PCD), it is the best material to be used for milling tools [3]. However, it is difficult to produce such milling tools in a productive way due to its veryhigh hardness and wear resistance. Although electrical discharge machining (EDM) is known to be one of the most practical ways for machining hard materials, it is not applicable for BLPCD due to its electric non-conductance [4]. A method utilizing a reaction between diamond and iron may be applied [5]. The productivity, however, may not be satisfactory.

This paper investigates the feasibility of machining BLPCD by laser both by physical experiment and by numerical simulation and the applicability of laser machining for mass production of BLPCD tools is evaluated. The laser used in the study was the femtosecond pulsed laser (FSPL) expecting the excellent surface quality to be generated by the ablation effect of FSPL [6,7]. Also, the differences between the surfaces machined by FSPL and surfaces machined by nanosecond pulsed laser (NSPL) were comparatively studied.

2. Experiment setup and procedures

The experimental study was performed by using FSPL and NSPL. Table 1 shows the major parameters of the lasers used. The BLPCD tool blanks (diameter: 1.2 mm, thickness 0.65 mm) shown in Fig. 1(a), were used in the experiments. Fig. 1(b) shows the experimental setup when the tool blank was machined by FSPL. Fig. 1(c) shows the entire view of the work bench with laser beam used for the experiments. The laser beam power and polarization was adjusted by optical attenuator and half and quarter wave plates and then the beam was guided by dielectric mirrors to galvanometer scanner to generate the scanning beam, which moves at more than 1 m/s speed in *X*–*Y* plane. The work bench has four-axis (XYZ linear and *B* axis rotary).

In the experiments, two types of laser beam irradiation against the BLPCD target were used. One type is so-called "normal irradiation" in which the laser beam was irradiated normal to the

Table 1
Typical parameters of lasers used in the experiments.

	FSPL [8]	NSPL [9]
Pulse width	350 fs	140 ns
Wavelength	1045 nm (IR) 522 nm (SHG)	1064 nm
Pulse repetition rate	200 kHz	10–100 kHz
Focal spot diameter	40 μm (IR) 20 μm (SHG)	40 μm
Average power	<10 W	<100 W
Pulse energy	<50 μJ	<1000 μJ

* Corresponding author. Tel.: +15308671178.
E-mail address: kyamazaki@ucdavis.edu (K. Yamazaki).

http://dx.doi.org/10.1016/j.cirp.2016.04.081
0007-8506/

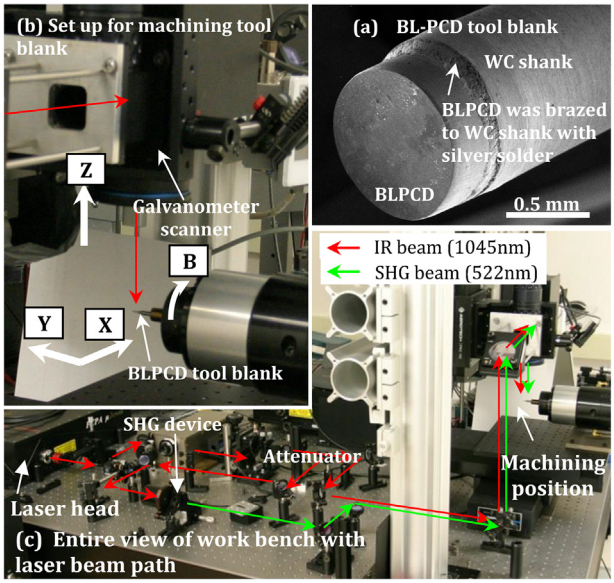

Fig. 1. Views of work bench for experiments.

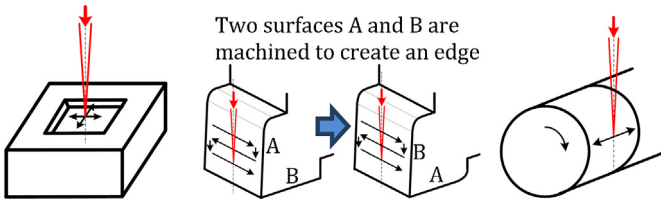

Fig. 2. Schematics of 3 types of laser machining methods for fabrication of BLPCD tool.

Table 2
Targeted productivity and quality for BLPCD micro ball end mill.

Material removal rate	>0.001 mm^3/s
Surface roughness Ra	Roughing process < 0.3 μm Finishing process (Edge formation) < 0.05 μm
Edge sharpness	<R1 μm
Post process after laser machining	No or minimum post processing by electrolysis for removing thin graphitized layer if it exists.

surface to be machined. The other type is referred to as "parallel irradiation", where the laser beam is irradiated in the parallel direction to the surface to be machined by using the side of the beam. "Parallel irradiation" has been known as "laser grinding" to polish the surface of hard materials [10]. By selectively using one of these two types irradiation, experiments have been carried out by machining three types of primitive geometries. These are pocketing, sharp edge creation and cylindrical turning respectively as shown in Fig. 2. These three types of geometry primitive were chosen by considering the necessary local geometries to be formed in the typical micro milling tool. "Pocketing" is mainly used to cut large part of BLPCD tool blank by "normal irradiation" of the beam. "Edge creation" is to be used for creating the sharp cutting edge by "parallel irradiation". "Cylindrical turning" is to finish the outer cylindrical surface by "parallel irradiation" in the vicinity of cutting edge. Table 2 shows the typical productivity and quality target for mass-production of the micro ball end mill made of BLPCD based on our internal survey.

3. Experimental results

3.1. MRR and surface roughness obtained by normal irradiation of NSPL and FSPL

In the experiments, the first, the material removal rate (MRR) and obtained average surface roughness (Ra) when machining a pocket on BLPCD by NSPL and FSPL normal irradiation were evaluated. Both lasers were IR. The target MRR was set to more

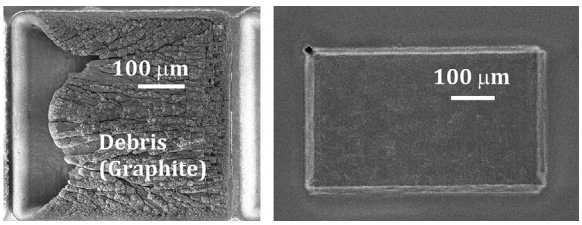

Fig. 3. Machined surfaces obtain by (a) NSPL (average power: 6 W) and (b) FSPL (average power: 5 W) normal irradiation.

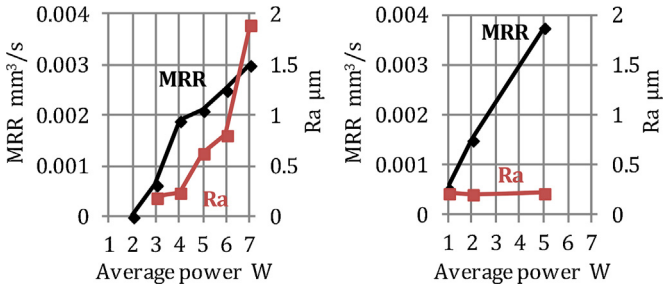

Fig. 4. Comparison of average surface roughness Ra and MRR by NSPL and FSPL. Pulse pitch: 2 μm constant.

than 0.001 mm^3/s. With this MRR, the diameter 1.0 mm ball end mill can be fabricated from 1.2 mm diameter cylindrical BLPCD tool blank and machining time is about 10 min.

Fig. 3 shows the machined surface observed by SEM. When machining by NSPL with average power more than 6 Watts, a lot of debris or re-solidified materials left on the machined surface as shown in Fig. 3(a), while they were not observed on the surface machined by FSPL as shown in Fig. 3(b). The re-solidified problem became even severer as higher average power NSPL was applied and limited the maximum speed. Fig. 4 shows the relationship of MRR and surface roughness Ra with respect to laser average power. Ra was measured after removing debris left on the surface.

Although the targeted MRR could be achieved by both NSPL and FSPL, the targeted surface roughness Ra could only be achieved with FSPL. Ra stayed within 0.3 μm range regardless of the laser power as shown in Fig. 4(b). As a result, it has been concluded that required both MRR and surface roughness for rough machining of BLPCD can be achieved only by FSPL.

3.2. High quality surface generation by parallel irradiation of FSPL

Since the best surface roughness Ra with normal irradiation with FSPL was 0.2 μm, which is not satisfactory for quality required for finishing the BLPCD surface, machining experiments by FSPL parallel irradiation were conducted. It is a well-known fact that irradiating the laser beam parallel to the surface to be machined is effective to improve the surface quality [10]. The experiments were performed by two types of polarization and two kinds of laser wavelength. Fig. 5 shows the machined surfaces observed by SEM. As shown in Fig. 5(a), the surface machined by IR FSPL with linear polarization clearly indicated the laser induced periodic surface structure (LIPSS). It is a typical phenomenon observed when the surface is machined by FSPL [11]. It is known that the LIPSS varies depending on polarization and wavelength [12,13]. When the circular polarization IR FSPL was used, the LIPSS was almost invisible resulting in the improvement of Ra from 0.16 μm to 0.096 μm as shown in Fig. 5(a) and (b).

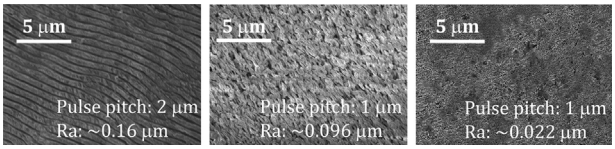

Fig. 5. SEM images of FSPL parallel-machined surface with (a) IR linear polarization, (b) IR circular polarization and (c) SHG circular polarization.

Please cite this article in press as: Ogawa Y, et al. A study on machining of binder-less polycrystalline diamond by femtosecond pulsed laser for fabrication of micro milling tools. CIRP Annals - Manufacturing Technology (2016), http://dx.doi.org/10.1016/j.cirp.2016.04.081

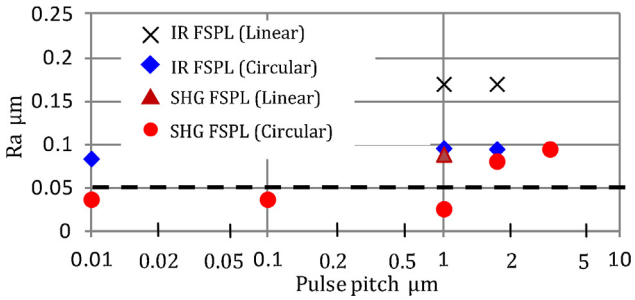

Fig. 6. Comparison of parallel processed surface roughness (Ra).

The best surface quality was achieved by using circular polarization SHG. The Ra was about 0.022 μm as shown in Fig. 5(c). Eventually, we successfully achieved target requirement specification for surface roughness of finishing (<0.05 μm). The pulse pitch dependence of Ra under the two types of laser and two types of polarization is summarized in Fig. 6.

The pulse pitch is defined with Eq. (1).

$$Pulse\ \ pitch = \frac{v_{scan}}{f_{PR}} \tag{1}$$

where v_{scan} is scan speed of laser (μm/s) and f_{PR} is pulse repetition rate (s^{-1}).

3.3. Sharp edge formation

Using the conditions found for highest surface quality, feasibility test of edge formation was performed and formed edge was measured by point autofocus measuring instrument [14]. Fig. 7(a) shows the 3D profile of the edge formed by FSPL. The sharpness of the edge is shown in Fig. 7(b). The sharpness of the edge was R0.8 μm. It satisfies target requirement (<R1.0 μm) given in Table 2.

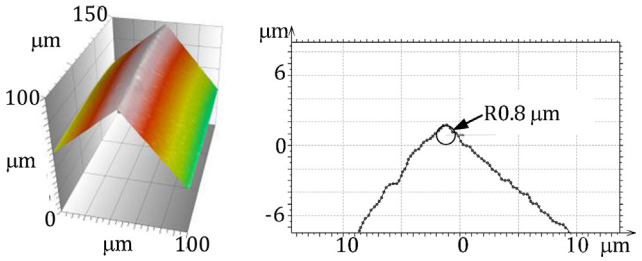

Fig. 7. Measured results of best finished edge by parallel FSPL with SHG irradiation.

3.4. Raman spectroscopy

Raman spectroscopy was used to evaluate the chemical state change after laser irradiation.

The measured spectra are shown in Fig. 8. In case of NSPL, large two peaks were observed at 1350 cm^{-1} and 1580 cm^{-1}. Those peaks correspond to the D-band and G-band of sp^2-bonded of graphite respectively. This indicates that the thermally induced graphitization process occurred by NSPL irradiation. The thickness of graphitic layer formed by NSPL was found to be 2–5 μm by comparison of the before and after the removal of graphitized layer by cleaning with acid. For the machined surface by FSPL, only diamond (1333 cm^{-1}) peak was observed. This result is consistent with the reference paper [16]. By considering the fact that the optical penetration depth of graphite for incident light used for the Raman spectroscopy (λ = 532 nm) is about 50 nm [15], the thickness of formed graphitic layer by FSPL machining was found to be much less than 50 nm.

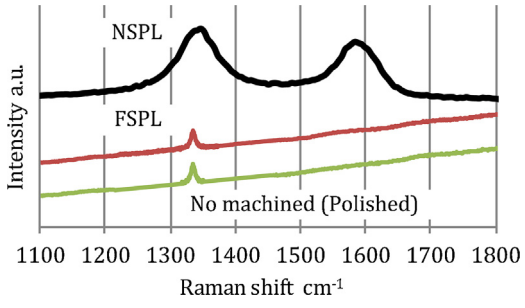

Fig. 8. Raman spectra after laser machining.

3.5. Rough tool shape formation

Using the machining conditions obtained from the experiments mentioned above, the feasibility study of the fabrication of BLPCD micro ball end mill was performed by machining the tool blank into the rough shape of ball end mill. Fig. 9(a) shows the shaped hemisphere generated by FSPL cylindrical turning. The roundness of the hemisphere was about 0.7 μm (Fig. 9(b)). Then, the top half portion was removed by FSPL normal irradiation and the rough shape of the ball end mill was obtained as shown in Fig. 9(c). Actual machining time to obtain the shape in Fig. 9(c) from the tool blank was about 20 min.

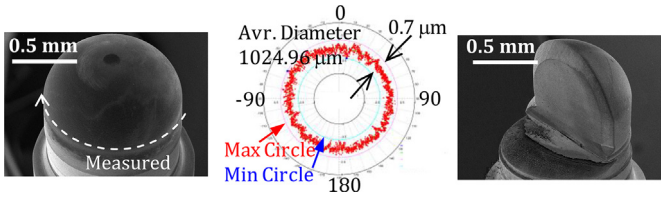

Fig. 9. (a) SEM image of hemispherical shape formed with FSPL, (b) Roundness of hemispherical shape measured along the line shown in (a), (c) SEM image of rough shape of ball end mill formed with FSPL.

4. Numerical simulation for dynamics of laser ablation

To establish a fundamental understanding of the laser ablation mechanism of BLPCD, a two dimensional Finite Difference Time Domain (FDTD) numerical scheme was adopted for the analysis. The detail of scheme is available in the paper by Zohdi [17].

The governing equation to be solved is the first law of thermodynamics;

$$\rho\dot{\omega} = -\nabla\cdot\mathbf{q} + \rho z \tag{2}$$

where z is a source term, θ, the temperature, and $\omega = \rho c\theta$, the internal energy. The heat flux, $\mathbf{q}$, is given by Fourier's law, (3)

$$\mathbf{q} = -\mathbf{K}\nabla\theta \tag{3}$$

where $\mathbf{K}$ is the material conductivity. A Beer–Lambert scheme is used to model the intensity of the laser pulse at a laser depth, x^*, for a given absorption coefficient, a;

$$I(x) = I_0 e^{-\int_0^{x^*} adx} \tag{4}$$

Ablation is modelled via a reduction of material density governed through a rate equation,

$$\dot{\rho} = -C_{abl}\left(\frac{\theta}{\theta_{abl}}\right) \quad for\ \ \theta > \theta_{abl} \tag{5}$$

where C_{abl} is a rate parameter, and θ_{abl} the ablation temperature. Material properties are then scaled by the ratio of reduced density to un-ablated density. Graphitization is modelled using a similar rate equation however, to allow for a more direct comparison of the two lasers, the thermally stimulated graphite region was only tracked and the material properties in the region were not modified.

Please cite this article in press as: Ogawa Y, et al. A study on machining of binder-less polycrystalline diamond by femtosecond pulsed laser for fabrication of micro milling tools. CIRP Annals - Manufacturing Technology (2016), http://dx.doi.org/10.1016/j.cirp.2016.04.081

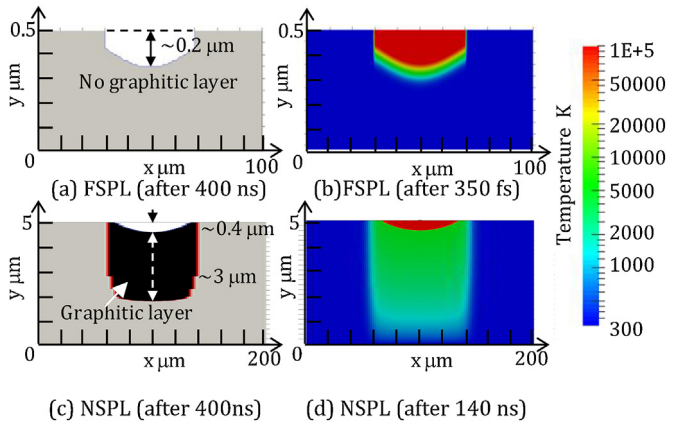

Fig. 10. Comparison of the ablation and graphitic region after 400 ns (left) and temperature distribution (right) after laser irradiation (FSPL: 350 fs, NSPL: 140 ns) between (a and b) FSPL and (c and d) NSPL.

As BLPCD is a relatively new material, the correct absorption coefficients for FSPL or NSPL are not well known. To determine appropriate values, simulations with various absorption coefficients were executed using the laser parameters used in the experiments until the simulation results approximately matched with experimental results for ablation depth and graphite formation depth. For FSPL, an absorption coefficient of $8 \times 10^7\ m^{-1}$ gave results consistent with the experiments. The high absorption coefficient for FSPL can be explained by a combined effect of multi-photon and excited state absorption. During a FSPL pulse, laser absorption initially occurs through multi-photon absorption mechanisms. The time scale at which this absorption occurs however creates a state of high-density electron excitation, greatly increasing the absorption coefficient of the material [18,19]. For NSPL, the absorption coefficient was also estimated to be $8 \times 10^7\ m^{-1}$. It is similar to the absorption for highly oriented pyrolytic graphite (HOPG) [20]. This can be explained by the occurrence of thermally stimulated graphitization during the relatively longer pulse duration.

Using the determined absorption values, a comparison between a nanosecond (t = 140 ns) and femtosecond (t = 350 fs) duration pulse was performed. The laser energies, chosen to match the values used in the physical experiment, were 25 μJ and 500 μJ for FSPL and NSPL with a Gaussian beam profile. The thermally stimulated graphite region formation was tracked but the material properties in the region were not modified to simplify the comparison of the two lasers.

Fig. 10 shows the thermal distribution and graphitization/ablation area after laser irradiation by FSPL and by NSPL. Here, it is assumed that ablation of diamond occurs when the maximum temperature reaches more than 4800 K [21], and graphitization occurs when the temperature stays between 2000 K [20] and 4800 K. Because the ablation temperature of the diamond is not clear, we assumed it from the phase diagram of carbon and the reference [21]. In the case of FSPL, the laser supplies all its energy before thermal diffusion begins, which results in the ablation without any graphitization. In the NSPL case, heat diffusion occurs in-time with the pulse resulting in lower peak temperatures and the formation of a graphitization layer at both the bottom and side walls. Those results are consistent with experimental results obtained by Raman spectroscopy mentioned in Section 3. In both cases, lateral temperature distribution is due to purely thermal diffusion and vertical one is due to both optical penetration and thermal diffusion. The dependence of graphite formation on laser pulse energy for FSPL was also investigated. For increasing energy levels, very little changes in graphite formation occurs for the FSPL case while for the NSPL case greater, more dispersed graphite and ablation zones are noted. This implies increasing the power for the FSPL will lead to increased MRR with no significant increase in the size of the graphitization.

5. Conclusion

Aiming at mass-produce of high performance micro milling tools made of BLPCD (binder-less polycrystalline diamond), machining of BLPCD by nanosecond and femtosecond pulse lasers was comparatively studied by experiments as well as by simulation with numerical analysis approach. It turned out that the femtosecond pulse laser with circular polarization is the best laser for successful machining of BLPCD resulting in 0.022 μm average surface roughness with almost no graphitization surface layer and almost 0.004 mm^3/s material removal rate.

References

[1] Irifune T, Kurio A, Sakamoto S, Inoue T, Sumiya H (2003) Ultra-Hard Polycrystalline Diamond from Graphite. *Nature* 421:599–600.
[2] Sumiya H (2012) Novel Development of High-Pressure Synthetic Diamond "Ultra-Hard Nano-Polycrystalline Diamond". *SEI Technical Review No 74* 15–23.
[3] Harano K, Satoh T, Sumiya H (2012) Cutting Performance of Nano-Polycrystalline Diamond. *Diamond & Related Materials* 24:78–82.
[4] Morgan C-J, Vallance R-R, Marsh E-R (2004) Micro Machining Glass With Polycrystalline Diamond Tools Shaped by Micro Electro Discharge Machining. *Journal of Micromechanics and Microengineering* 12:1687–1692.
[5] Shimada S, Tanaka H, Higuchi M, Yamaguchi T, Honda S, Obata K (2004) Thermo-Chemical Wear Mechanism of Diamond Tool in Machining of Ferrous Metals. *Annals of the CIRP* 53(1):57–60.
[6] Momma C, Nolte S, Chichkov B-N, Alvensleben F-V, Tunnermann A (1997) Precise Laser Ablation With Ultrashort Pulses. *Applied Surface Science* 109–110:15–19.
[7] Okuchi T, Ohfuji H, Odake S, Kagi H, Nagatomo S, Sugata M, Sumiya H (2009) Micromachining and Surface Processing of the Super-Hard Nano Polycrystalline Diamond by Three Types of Pulsed Lasers. *Applied Physics A* 96:833–842.
[8] http://www.imra.com/products/product-lines/fcpa-microjewel.
[9] http://en.dmgmori.com/products/lasertec/lasertec-precisiontool/lasertec-20-precisiontool.
[10] Suzuki D, Itoigawa F, Kawata K, Suganuma T, Nakamura T (2012) Edge Sharpening and Surface Modification of PcBN Cutting Tool by Pulsed Laser Grinding. *Key Engineering Materials* 523–524:131–136.
[11] Li L, Hong M, Schmidt M, Zhong M, Malshe A, Huis in't Veld B, Kovalenko V (2011) Laser Nano-Manufacturing – State of the Art and Challenges. *Annals of the CIRP* 60(2):735–755.
[12] Gräf S, Müller F-A (2015) Polarisation-Dependent Generation of fs-Laser Induced Periodic Surface Structures. *Applied Surface Science* 331:150–155.
[13] Golosov E-V, Ionin A-A, Kolobov Y-R, Kudryashov S-I, Ligachev A-E, Novoselov Y-N, Seleznev L-V, Sinitsyn D-V (2011) Ultrafast Changes in the Optical Properties of a Titanium Surface and Femtosecond Laser Writing of One-Dimensional Quasi-Periodic Nanogratings of its Relief. *Journal of Experimental and Theoretical Physics* 113(1):14–26.
[14] Leach L (2011) *Optical Measurement of Surface Topography*, Springer: 107–128.
[15] Palik E-D (1997) *Handbook of Optical Constants of Solids 2*.
[16] Ozkan A-M, Malshe A-P, Railkar T-A, Brown W-D (1999) Femtosecond Laser-Induced Periodic Structure Writing on Diamond Crystals and Microclusters. *Applied Physics Letters* 75(23):3716–3718.
[17] Zohdi T-I (2015) Modeling and Simulation of Laser Processing of Particulate-Functionalized Materials. *Archives of Computational Methods in Engineering* 1–25. http://dx.doi.org/10.1007/s11831-015-9160-1.
[18] Jiang L, Tsai H-L (2005) Energy Transport and Material Removal in Wide Bandgap. *International Journal of Heat and Mass Transfer* 48:487–499.
[19] Rublack T, Seifert G (2011) Femtosecond Laser Delamination of Thin Transparent Layers from Semiconducting Substrates. *Optical Materials Express* 1(4):543–550.
[20] Kononenko V-V, Kononenko T-V, Pimenov S-M, Sinyavskii M-N, Konov V-I, Dausinger F (2005) Effect of the Pulse Duration on Graphitization of Diamond During Laser Ablation. *Quantum Electronics* 35(3):252–256.
[21] Savvatimskiy A-I (2005) Measurements of the Melting Point of Graphite and the Properties of Liquid Carbon (a Review for 1963–2003). *Carbon* 43:1115–1142.

Please cite this article in press as: Ogawa Y, et al. A study on machining of binder-less polycrystalline diamond by femtosecond pulsed laser for fabrication of micro milling tools. CIRP Annals - Manufacturing Technology (2016), http://dx.doi.org/10.1016/j.cirp.2016.04.081